

## MIT Open Access Articles

*Thermal interface conductance in Si/Ge superlattices by equilibrium molecular dynamics*

The MIT Faculty has made this article openly available. **Please share** how this access benefits you. Your story matters.

**Citation:** Chalopin, Y. et al. "Thermal Interface Conductance in Si/Ge Superlattices by Equilibrium Molecular Dynamics." Physical Review B 85.19 (2012). ©2012 American Physical Society

**As Published:** <http://link.aps.org/doi/10.1103/PhysRevB.85.195302>

**Publisher:** American Physical Society

**Persistent URL:** <http://hdl.handle.net/1721.1/79797>

**Version:** Final published version: final published article, as it appeared in a journal, conference proceedings, or other formally published context

**Terms of Use:** Article is made available in accordance with the publisher's policy and may be subject to US copyright law. Please refer to the publisher's site for terms of use.



# Thermal interface conductance in Si/Ge superlattices by equilibrium molecular dynamics

Y. Chalopin,<sup>1,2</sup> K. Esfarjani,<sup>2</sup> A. Henry,<sup>3</sup> S. Volz,<sup>1</sup> and G. Chen<sup>2</sup>

<sup>1</sup>*Laboratoire d'Energétique Moléculaire et Macroscopique, CNRS UPR 288, Ecole Centrale Paris, F-92295 Châtenay-Malabry, France*

<sup>2</sup>*Mechanical Engineering Department, Massachusetts Institute of Technology, Cambridge, Massachusetts 02139, USA*

<sup>3</sup>*George W. Woodruff School of Mechanical Engineering, Georgia Institute of Technology,  
771 Ferst Drive Atlanta, Georgia 30332-0405, USA*

(Received 22 October 2011; revised manuscript received 13 February 2012; published 1 May 2012)

We provide a derivation allowing the calculation of thermal conductance at interfaces by equilibrium molecular dynamics simulations and illustrate our approach by studying thermal conduction mechanisms in Si/Ge superlattices. Thermal conductance calculations of superlattices with period thicknesses ranging from 0.5 to 60 nm are presented as well as the temperature dependence. Results have been compared to complementary Green-Kubo thermal conductivity calculations demonstrating that thermal conductivity of perfect superlattices can be directly deduced from interfacial conductance in the investigated period range. This confirms the predominant role of interfaces in materials with large phonon mean free paths.

DOI: [10.1103/PhysRevB.85.195302](https://doi.org/10.1103/PhysRevB.85.195302)

PACS number(s): 65.40.-b, 65.80.-g, 44.10.+i, 44.05.+e

## I. INTRODUCTION

In recent years, interfacial thermal transport has become a major subject of interest<sup>1,2</sup> with regard to two important technological applications, namely, thermoelectric materials development<sup>3</sup> and microelectronics thermal management. Thermoelectric materials require low thermal conductivity, which may be potentially tuned by nanoscale interfaces between dissimilar crystalline materials on one hand<sup>4</sup> and grain boundaries on the other hand. Here the objective is to lower the overall thermal conductivity by increasing the number of low conductance interfaces. In the case of microelectronics, the devices are typically constructed from many layers of different materials and the interfacial thermal resistance impedes the removal of heat. Here, the goal is to increase the interfacial conductance so that heat generated by the Joule effect can be removed and the package can be cooled more effectively.<sup>5</sup> Thermal properties of such nanostructures are generally strongly influenced by phonon scattering at boundaries and interfaces and a fundamental understanding of the atomic level physics that governs the interfacial conductance is needed.<sup>6-8</sup> In addition, heat transfer in nanomaterials is strongly impacted by the presence of defects (vacancies, dislocations, impurities, etc.), which generate supplementary phonon scattering in the material. Consequently, two important questions arise regarding heat conduction in solids including interfaces: first, what is the contribution of interfacial scattering compared to that of internal phonon-phonon scattering, and second, what are the mechanisms of interfacial transmission of the vibrational modes? Extensive modeling of this contact resistance has brought to light two models,<sup>9</sup> namely, the acoustic mismatch model, assuming a single direction of transmission and of reflection, and the diffuse model, which considers equiprobable scattering directions. These two models remain, however, incomplete and since thermal conductance has been widely studied by several complementary numerical approaches such as the Boltzmann transport equation, molecular dynamics (MD) simulations, atomistic Green's function (AGF) methods<sup>10-12</sup> [also referred to as nonequilibrium Green's function (NEGF)], and first-principle calculations. Each of these methods has

advantages and disadvantages but our discussion will be restricted to MD simulations recalling that these are based on solving the classical dynamics of  $N$ -body systems and are thus particularly well suited for recovering statistical properties (e.g., response functions, thermodynamics properties, etc.). MD calculations of thermal conductance currently rely on a nonequilibrium approach where a constant heat flux is fixed across the system<sup>13-17</sup> through two thermal reservoirs obtained with local velocity rescaling. As a result, a temperature drop can be estimated at the interface region, allowing the estimation of thermal conductance. Although this procedure is direct and relatively convenient to implement, it excludes periodic boundary problems and suffers from disadvantages. Constant rescaling of the atomic velocities in the thermostats introduces artificial scattering and, consequently, the number of atomic layers forming the separation distances between the reservoirs and the characteristic time of the thermostats are critical parameters. We propose a microscopic approach for calculating thermal conductance at interfaces based on the tracking of equilibrium fluctuations, which presents analogies with the well-know Green-Kubo (GK) method<sup>18</sup> for thermal conductivity.<sup>19</sup> Sections II and III provide a rigorous derivation of the thermal conductance revealing a clear physical picture of thermal interfacial transport. We develop how such a calculation can be implemented in MD and how to properly compute thermal conductance at thermal equilibrium. In Sec. IV, we study the thermal conductance mechanisms of Si/Ge superlattices at various temperatures and with various period thicknesses. Further comparison with Green-Kubo thermal conductivity calculations shows that it can be directly deduced from the sum of the interface resistances in perfect lattices with periods exceeding 2 nm.

## II. THEORY OF INTERFACE CONDUCTANCE AT THERMAL EQUILIBRIUM

In the following, we considered two systems,  $A$  and  $B$ , in thermal interaction at the same equilibrium temperature. The total Hamiltonian can be written as  $H = H_A + H_B$ , with  $H_A$  and  $H_B$  being defined from a local energy at each atomic site

as follows:

$$H_{A/B} = \sum_{i \in A/B} h_i = \sum_{i \in A/B} \frac{p_i^2}{2m_i} + V_i, \quad (1)$$

where  $p_i$  and  $m_i$  refer to the atom  $i$ 's momentum and mass, respectively. In the case of pair potential interactions, for instance,  $V_i = \sum_{j \neq i} V(r_i - r_j)/2$  and exactly half of the interaction term belongs to  $H_A$  and the other half to  $H_B$ .

To obtain the interfacial thermal conductance, we use the linear response formalism<sup>20</sup> where an infinitesimally small temperature difference is applied between systems  $A$  and  $B$ . This latter temperature difference,  $\Delta T = T_B - T_A$ , is sufficiently small that temperatures  $T_A$  and  $T_B$  in systems  $A$  and  $B$  are uniform and those latter systems are considered as thermal reservoirs. In the general case,  $T_A = T - \lambda \Delta T$  and  $T_B = T + (1 - \lambda) \Delta T$  with  $0 < \lambda < 1$ . We further assume that the system  $A + B$  is insulated and its total energy  $E_A + E_B = \text{constant}$ .

The key simplifying assumption in our derivation is the assumption of the ‘‘quasiequilibrium’’ form of the nonequilibrium distribution function as

$$\rho = \frac{e^{-\beta_A H_A - \beta_B H_B}}{Z} \quad (2)$$

$$= \frac{e^{-\beta H} [1 - \beta H_{\text{field}} + O(\beta^2 H_{\text{field}}^2)]}{\text{Tr} e^{-\beta H} [1 - \beta H_{\text{field}} + O(\beta^2 H_{\text{field}}^2)]}. \quad (3)$$

In the classical case, the trace has to be understood as  $\text{Tr} A = \int d\mathbf{p} d\mathbf{q} A(\mathbf{p}, \mathbf{q})$ . The above  $H_{\text{field}}$  term actually defines the perturbation Hamiltonian, which can be obtained assuming a small  $\Delta T$  and using a Taylor expansion of the distribution function. The justification for such a nonequilibrium distribution is provided by Mori *et al.*<sup>21</sup>

The expression of the perturbation Hamiltonian resulting from the applied temperature difference is

$$H_{\text{field}} = [\lambda H_A - (1 - \lambda) H_B] \Delta T / T. \quad (4)$$

One can intuitively understand the above result by noting that the temperature difference is the quantity which ‘‘pulls’’ the energy up or down ( $\Delta T / T$  is the thermodynamic variable conjugate to energy).

Under a perturbation field, the expectation value of any operator  $Q$  becomes  $\langle Q \rangle = \text{Tr} \rho Q$ .  $\rho$  is the nonequilibrium distribution function defined just above yielding

$$\langle Q \rangle = (q - \beta \langle Q H_{\text{field}} \rangle) / (1 - \beta \langle H_{\text{field}} \rangle) \quad (5)$$

$$= q - \beta \langle Q H_{\text{field}} \rangle + \beta q \langle H_{\text{field}} \rangle + O(\beta^2 H_{\text{field}}^2), \quad (6)$$

where  $q = \text{Tr} \rho_o Q$  is the equilibrium expectation value of  $Q$ . Therefore  $\langle Q \rangle - q = -\beta [\langle Q H_{\text{field}} \rangle - q \langle H_{\text{field}} \rangle]$ . Substituting  $H_{\text{field}}$  with its expression in Eq. (4), we have

$$\langle Q \rangle = \beta \frac{\Delta T}{T} \langle Q [-\lambda H_A + (1 - \lambda) H_B] \rangle, \quad (7)$$

where the average on the right-hand side is with respect to the *equilibrium distribution*. The constant  $q$  maybe reabsorbed in the definition of  $Q$  so that its thermal equilibrium average is zero.

The static response function  $\chi_o$  to the applied temperature difference is defined by  $\langle Q \rangle = \chi_o \Delta T$ , and taking the parameter  $\lambda = 0$  provides the relationship between the static response

and (*equal-time*) correlations in the system:

$$\chi_o = \frac{\langle Q H_B \rangle}{k_B T^2}. \quad (8)$$

Setting  $Q = \dot{H}_A$  allows us to find out how much heat is added to the subsystem  $A$  per unit time when a temperature difference  $\Delta T$  is applied between  $A$  and  $B$ . Using the adiabatic condition  $\langle H_A + H_B \rangle = \text{constant}$  implies that any other choice of  $\lambda$  will lead to the same result.

The definition of the thermal conductance  $\mathcal{G}$  between systems  $A$  and  $B$ ,

$$\frac{d \langle H_A \rangle}{dt} = \mathcal{G} \Delta T, \quad (9)$$

combined with Eq. (8) provides

$$\mathcal{G} = \frac{1}{k_B T^2} \left\langle \frac{d H_A(t)}{dt} H_B(t) \right\rangle. \quad (10)$$

The derivative needs to be evaluated at the same time as  $H_B$  is evaluated, since we are dealing with an equal-time correlator. As such, it seems that the numerical computation of  $\mathcal{G}$  would require very little time, just enough to do a proper ensemble average in order to reduce the statistical errors below a specified threshold value. This is in contrast to the usual GK formula<sup>19</sup> which involves a time integral and also needs to be time and ensemble averaged. We can also derive a more familiar-looking formula by considering  $H_B(t) = \int_{-\infty}^t \dot{H}_B(t') dt'$ . Using the change of variable  $t' = t - \tau$ , we can then reexpress the thermal conductance as the time integral over the dissipated power correlator:

$$\mathcal{G} = \frac{1}{k_B T^2} \int_{-\infty}^t \langle \dot{H}_A(t) \dot{H}_B(t') \rangle dt' \quad (11)$$

$$= -\frac{1}{k_B T^2} \int_0^\infty \langle \dot{H}_A(t) \dot{H}_B(t - \tau) \rangle d\tau$$

$$= -\frac{1}{k_B T^2} \int_0^\infty \langle \dot{H}_A(0) \dot{H}_B(-\tau) \rangle d\tau \quad (12)$$

$$= -\frac{1}{k_B T^2} \int_0^\infty \langle \dot{H}_A(\tau) \dot{H}_B(0) \rangle d\tau \quad (13)$$

$$= \frac{1}{k_B T^2} \int_0^\infty \langle \dot{H}_A(\tau) \dot{H}_A(0) \rangle d\tau, \quad (14)$$

which looks like the usual GK formula. In the above derivation, we have assumed time-translational invariance, energy conservation,  $\dot{H}_B = -\dot{H}_A$ , and used  $\dot{H}_B(t') = -\dot{H}_B(t - \tau)$ , where the time derivative in the left term is with respect to  $t'$  and in the right term it is with respect to  $\tau$ .

An alternative formula, similar to the one often used for the diffusion coefficient can also be proved in this case:

$$\mathcal{G} = \frac{1}{k_B T^2} \lim_{t \rightarrow \infty} \frac{\langle [H_A(t) - H_A(0)]^2 \rangle}{2t}. \quad (15)$$

The usage of this form also requires long simulation times until the right-hand side converges to a constant value. Therefore, it seems that the use of Eq. (10) would be computationally more advantageous, and the conductance can be calculated within a canonical ensemble, requiring just an ensemble average over

uncorrelated equilibrium configurations generated even with a thermostat.

### III. IMPLEMENTATION FOR MOLECULAR DYNAMICS SIMULATIONS

#### A. Use of equations of motion to compute interfacial conductance

It is possible to obtain a direct method for computing thermal conductance of atomic systems with many degrees of freedom by considering the Hamiltonian equations of motion to express the time derivative of  $H_A$ :

$$\frac{dH_A(t)}{dt} = \sum_{i \in A \cup B} \left( \frac{\partial H_A}{\partial p_i} \dot{p}_i + \frac{\partial H_A}{\partial q_i} \dot{q}_i \right),$$

but

$$\dot{p}_i \equiv -\frac{\partial H}{\partial q_i} = F_i^A + F_i^B, \quad (16)$$

$$\dot{q}_i \equiv \frac{\partial H}{\partial p_i} = \frac{p_i}{m_i} = v_i, \quad (17)$$

$$\frac{\partial H_A}{\partial q_i} = -\left(F_i^A + \frac{1}{2}F_i^B\right) \text{ for } i \in A, \quad (18)$$

$$\frac{\partial H_A}{\partial q_i} = -\frac{1}{2}F_i^A \text{ for } i \in B, \quad (19)$$

$F_i^S$  being the force from the side  $S$  on atom  $i$ . The last two equations carry a factor of 1/2 because half of the  $A$ - $B$  interaction energy in  $H_A$  and the other half in  $H_B$  have been included [see the line following Eq. (1)]. Finally,

$$\frac{dH_A(t)}{dt} = \frac{1}{2} \left[ \sum_{i \in A} v_i F_i^B - \sum_{j \in B} F_j^A v_j \right], \quad (20)$$

which is the net power (or heat flux) absorbed by system  $A$ . Considering pairwise interactions, the net power simplifies to

$$\frac{dH_A(t)}{dt} = \frac{1}{2} \left[ \sum_{i \in A; j \in B} v_i - \nabla_i V(r_{ij}) - \nabla_j V(r_{ij}) v_j \right] \quad (21)$$

$$= - \sum_{i \in A; j \in B} \frac{(v_i + v_j)}{2} \nabla_i V(r_{ij}). \quad (22)$$

We should note that if  $A$  and  $B$  are strongly connected, the nonequilibrium molecular dynamics (NEMD) temperature drop will be smooth and span over the atoms linking  $A$  to  $B$ . The temperature difference will be, however, measured away from the interface atoms and deep into reservoirs  $A$  and  $B$ . The separation between  $A$  and  $B$  is in this case somewhat arbitrary, but the heat flux exchanged between  $A$  and  $B$  will always be the same in the steady state regardless of the choice of the  $A$ - $B$  boundary, and therefore the final thermal conductance should not depend on the latter. When studying near-field radiative transfer between dielectric nanoparticles, Dominguez *et al.*<sup>22</sup> also proposed to retrieve the conductance from equilibrium heat flux.

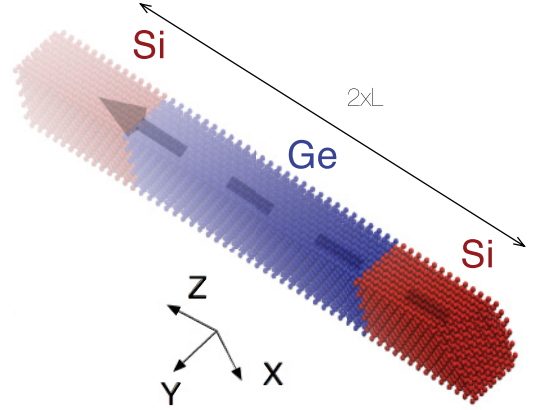


FIG. 1. (Color online) Spatial configuration of the superlattice junctions. Thermal conductance is investigated along direction  $Z$ .

#### B. Superlattice Si/Ge model for equilibrium molecular dynamics (EMD) simulations

In this work, we have implemented the three-body Stillinger-Weber interatomic potential<sup>23,24</sup> to reproduce the Si-Si and Ge-Ge covalent interactions. Potential parameters have also been combined according to the mixing rules described by Ref. 25 to model the interfacial Si-Ge interactions.

The structure is relaxed using a steepest descent energy minimization algorithm (sd). Atomic trajectories are then calculated in the NVE (microcanonical ensemble) ensemble with a time step of 1 fs. Thermal equilibrium has been achieved within 500 ps. Thermal conductance simulations have been operated on Si/Ge superlattices having a geometrical configuration similar to that presented in Fig. 1.

Heat conduction mechanisms are studied in the  $Z$  direction and periodic boundary conditions are applied in the three directions. This latter condition yields a Si/Ge interface of infinite cross section in the plane perpendicular to direction  $Z$  and involves a periodicity  $L_p = N(a_{\text{Ge}} + a_{\text{Si}})$  in the same direction, where  $a_{\text{Si/Ge}}$  stands for the lattice parameters and  $N$  is the number of unit cells. We included at least two contacts in the periodic supercell. We assume here a perfect interface between Si and Ge in which there is perfect lattice matching. This is often achieved through the introduction of coherency strain in one or both of the phases. The lattice parameter difference of 4% between Si (0.543 nm) and Ge (0.565 nm) has been matched to 0.554 nm in the direction perpendicular to the interface. This relaxation procedure has already been presented in various publications.<sup>26</sup> The resulting lattice parameters in the direction parallel to the contact correspond, respectively, to 0.531 and 0.573 nm for Si and Ge phases.

#### C. Retrieving thermal conductance from EMD simulations

Obtaining thermal conductance from equilibrium thermal fluctuations according to Eq. (14) requires large ensemble averages. In practice, tens of trajectories with different atomic random velocities distributions have to be considered to ensure an accurate prediction. Consequently, the thermal conductance is calculated through a two-step procedure.



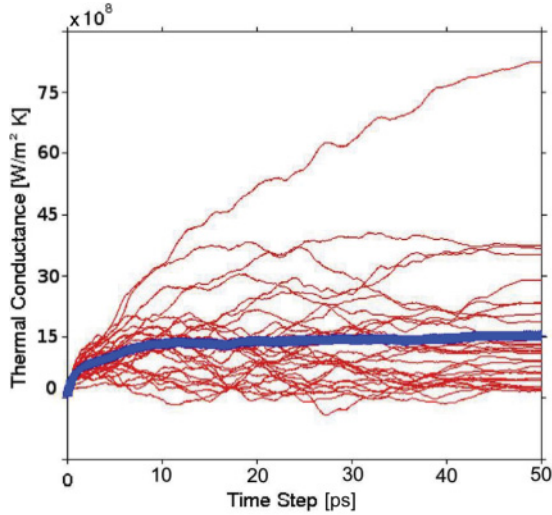


FIG. 2. (Color online) Thermal conductance obtained at 400 K for a superlattice with a period thickness of 40 nm with 30 independent runs. The average is plotted by the bold line.

(i) Several MD simulations are performed to capture the time-dependent fluctuations of the local net heat flux following Eq. (20) at a given equilibrium temperature.

(ii) The resulting averaged heat flux is then injected into Eq. (14) to retrieve the thermal conductance in a region where the integral of the autocorrelation has converged. Periodic boundary conditions are fixed in our calculation. From this, as one seeks to compute heat exchanges from Si to Ge, two contact surfaces  $S$  have to be considered. The resulting conductance calculated per unit square has then to be normalized by  $2S$ .

Figure 2 illustrates our methodology by reporting the thermal conductance obtained for a 40-nm period at 400 K with 30 independent runs. The number of ensemble average strongly depends on the junction cross section: enlarging the number of atoms forming the contact allows reducing the net heat flux fluctuations. The larger the contact surface is, the better the statistics is and ensemble averaging can be optimized. By considering now the resulting autocorrelation function (Fig. 3), it can be found that after a time ranging from 20 to 50 ps the correlation function reaches zero. As a result, we have considered autocorrelations of the net flux defined with  $2 \times 10^5$  net flux points sampled every 10 fs. The resulting integral is found to converge between 30 and 50 ps at 400 K. It is important to check that the convergence is ensured consistently by comparing the different conductance values obtained as a function of the number of trajectories for a given time-correlation length.

We first compared our approach with available data in the literature by simulating a single Si/Ge junction (2 slabs of 10 nm) with no periodic boundary conditions at 400 K. We found a thermal conductance of  $3.7 \text{ W/m}^2 \text{ K}$  which is similar to what has been recovered by Zhao and Freund<sup>27</sup> and Landry and McGaughey.<sup>28</sup> This validation allows us to focus on periodic systems in order to capture the relevant mechanism at play in Si/Ge superlattices.

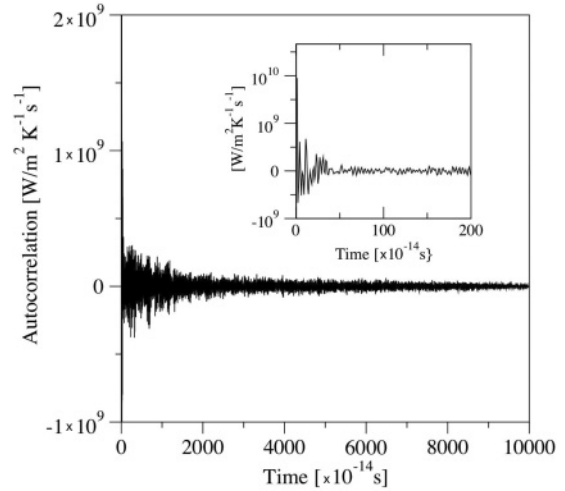


FIG. 3. Net heat flux autocorrelation function at 400 K. The inset shows a zoom of the 0- to 2-ps time interval.

#### IV. RESULTS FOR SI/GE SUPERLATTICES

##### A. Three-body vs two-body contribution to the interfacial heat flux

The three-body Stillinger-Weber potential<sup>23</sup> is one of the widely used empirical potentials for modeling atomistic properties of silicon and germanium. It has the particularity that pairwise interaction (two-body) occurs between the first nearest neighbors and another interaction that depends on the bonding angle between one atom of the unit cell and each of its second neighbors.

When considering the net flux computation, the interfacial interaction can be decomposed as a sum of two-body and three-body terms. Figure 4 shows a typical three-body interface configuration where atomic triplet  $i, j$ , and  $k$  forms an interface with  $i$  and  $j$  belonging to the same material but not  $k$ . In this particular illustrative example, when one assesses the different interface interactions, two-body contributions ( $F_{ik}$ ) as well as three-body contributions ( $F_j$  and  $F_k$ ) have to be included in the net flux estimation of (20).

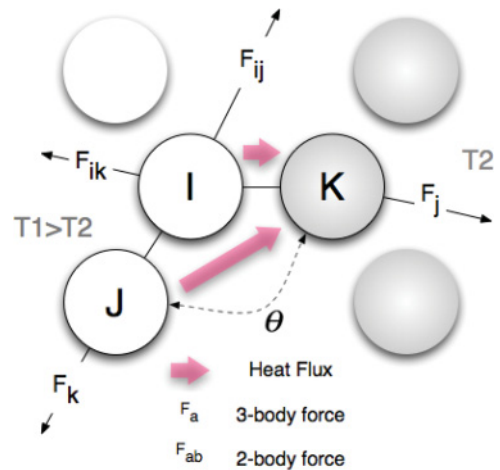


FIG. 4. (Color online) Interface configuration including two-body and three-body interactions. The three-body contribution to the net heat flux is expressed as  $Q_3 = \mathbf{f}_k \cdot \mathbf{v}_j - \mathbf{f}_j \cdot \mathbf{v}_k$ .

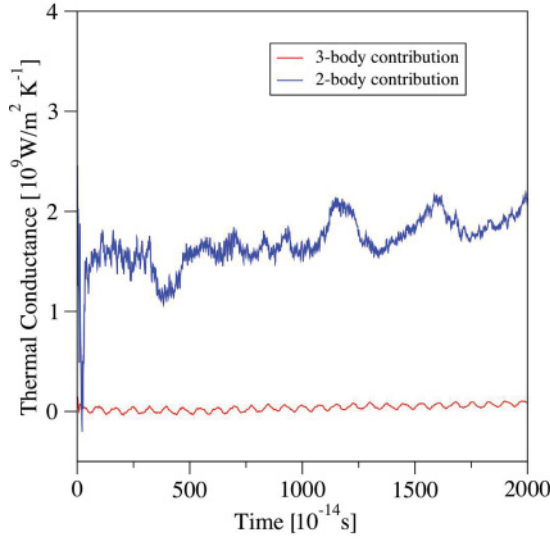


FIG. 5. (Color online) Three-body and two-body contributions to the thermal conductance of a double Si/Ge junction at 400 K. No ensemble averages have been considered here.

The method we proposed is general and can be applied to any potential. All that is needed is that the total system potential energy be written in terms of individual atom potential energy contributions. Essentially all potential forms can be rewritten in this format, even if the many-body terms have to be partitioned into thirds or fourths according to the atoms participating in the interaction. Here, the three-body contribution to the net flux between each triplet of atoms  $(i, j, k)$  depends on the definition of the interface, namely, the type of atoms involved in the evaluation of the interaction. As illustrated in Fig. 4, the three-body contribution to the net heat flux is expressed as  $Q_3 = \mathbf{f}_k \cdot \mathbf{v}_j - \mathbf{f}_j \cdot \mathbf{v}_k$ .

This raises the question of how each set of interactions contributes to the conductance. We report the contribution to the thermal conductance for these two types of interactions in Fig. 5. In fact, the three-body contribution does not contribute significantly to Si/Ge interfacial heat transfer which remains fully driven by pairwise two-body interaction forces. This result suggests that the interfacial phonon scattering occurs predominantly in the vicinity of the first Si/Ge pair of atomic layers forming the contact over a distance smaller than 0.2 nm. One can potentially tune interface conductance in a significant way by including atomic defects within these first atomic layers. It also reveals that any consistent numerical/experimental comparisons rely on a perfect knowledge of the atomic contact configuration.

### B. Temperature dependence of superlattice interface conductance

We calculated the thermal conductance of a Si/Ge superlattice with a layer thickness of 20 nm on a wide range of temperatures. This section aims at demonstrating the impact of anharmonicity at the interface. As inelastic processes occur at high temperatures, additional vibrational relaxation can be expected for phonon modes traveling at the interface. The coupling probability with compatible modes traveling on the other side of the junction can be influenced by the

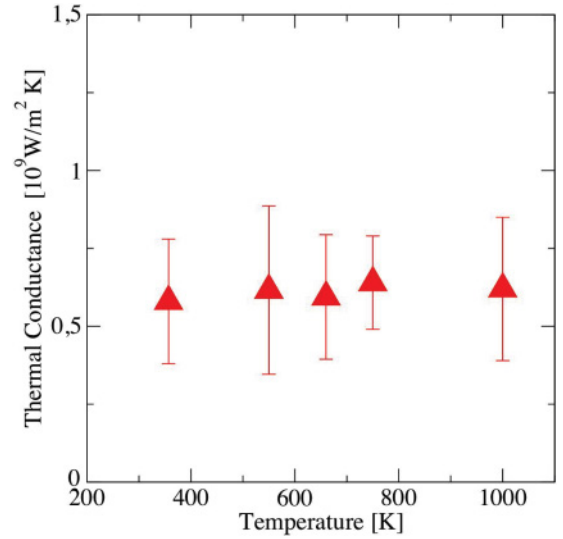


FIG. 6. (Color online) EMD thermal conductance predictions of a  $L_p = 20$  nm Si/Ge superlattice over 300 K to 1000 K.

local temperature. We performed this calculation according to the relaxation procedure describe in Sec. III. We found that conductance at interfaces is sensitive to the sample pressure and consequently it is important to monitor carefully the pressure obtained for the higher equilibrium temperatures to eventually relax the structure with additional runs in the isobaric-isothermal ensemble.

We reported (Fig. 6) the thermal interface conductance of superlattices over a temperature ranging from 300 K to 1000 K for a period of  $L_p = 20$  nm. Other work reported interesting results on a single interface.<sup>26,28</sup> Here, it can be seen that the temperature does not affect the conductance of the interface and clearly saturates around the value of  $\sim 0.75 \times 10^9$  W/m<sup>2</sup> K<sup>-1</sup>. Our calculations are performed in the classical approximation; equipartition of the thermal energy excludes any quantum effect in the phonon population. At the higher temperatures, it seems that phonon-phonon scattering is unlikely to occur for a 20-nm period. Other MD calculations of Si/Ge superlattice thermal conductivity tend to confirm this trend.<sup>29</sup> Note that this constant temperature is in contrast with previous NEMD calculations performed on individual Si/Ge/Si and Ge/Si/Ge junctions showing that resistance increases with increasing temperatures.<sup>26,28</sup>

This result is relevant to understand the dependence of the thermal conductivity of superlattices on the temperature: since interface resistance is not dependent on the temperature, any observed thermal conductivity change should result in the modification of the contribution of internal phonon-phonon scattering within the different layers forming the interface.

### C. Effect of period thickness on the thermal resistance of Si/Ge superlattices

In this section thermal conductances of Si/Ge superlattices with period thicknesses ranging from 0.54 to 60 nm are presented. An equilibrium temperature of 400 K is fixed as fair compromise between the high temperature approximation to which MD is bounded and the experimental thermal conductance measurements available in the literature. As can

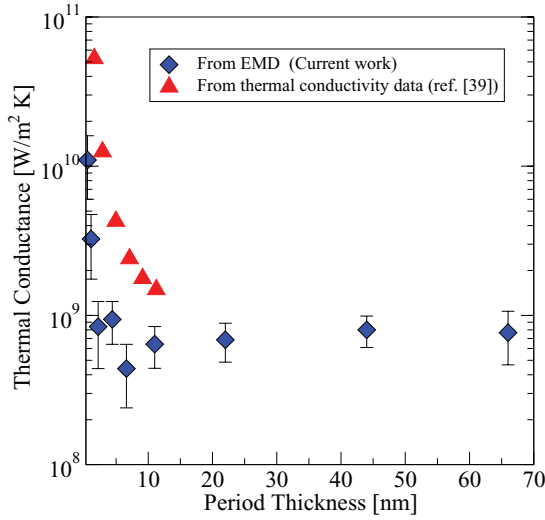


FIG. 7. (Color online) Computed interface thermal conductance  $G$  as a function of the period thickness. Comparison with data extracted from thermal conductivity<sup>30</sup>  $\lambda$  using  $\lambda = GL_p$ .

be seen in Fig. 6, thermal conductance decreases by about 1 order of magnitude when period thickness increases from 0.5 to 5 nm. Then, it remains constant over the full 5 to 60 nm range. Other NEMD calculations performed at small period thicknesses<sup>30</sup> also showed that superlattice thermal conductivity decreases with increasing period length. We extracted the corresponding thermal conductance  $G$  from  $\lambda/L_p$  and compared it to that obtained in the present work (Fig. 7). We covered here the cases where layer thicknesses approach and then exceed the characteristic length from which the contribution of evanescent modes eventually arises. Here, we define an evanescent mode as a nonpropagative surface mode that exists at the interface formed by the two layers and that is locally confined over a typical thickness. Note that in the range 300 K to 500 K, Si and Ge have dominant phonon mean free paths (MFPs) greater than 100 nm. Consequently, phonons travel ballistically in the individual Si and Ge layers and internal phonon-phonon scattering does not occur between contacts.<sup>31</sup>

Previous NEMD works have also shown that phonon transport in Ge/Si/Ge film is ballistic, while the phonon transport in Si/Ge/Si film of the same thickness is somewhat diffusive.<sup>32</sup> It would be interesting to address with our EMD approach the problem of the phonon transport in superlattices made of different Si and Ge layer thicknesses.

#### D. Further comparisons with Green-Kubo cross-plane thermal conductivity

Thermal transport models for semiconductor superlattices usually deal with two extreme cases. When the phonon MFP is much larger than the superlattices' period thicknesses, thermal conductivity is predicted from lattice dynamics.<sup>33</sup> On the contrary, when the phonon MFP is shorter than the superlattice period,<sup>31,34–36</sup> thermal conductivity is calculated using the Boltzmann transport equation (BTE). These models are, however, inefficient at predicting thermal properties of systems that are neither purely coherent nor purely diffusive.

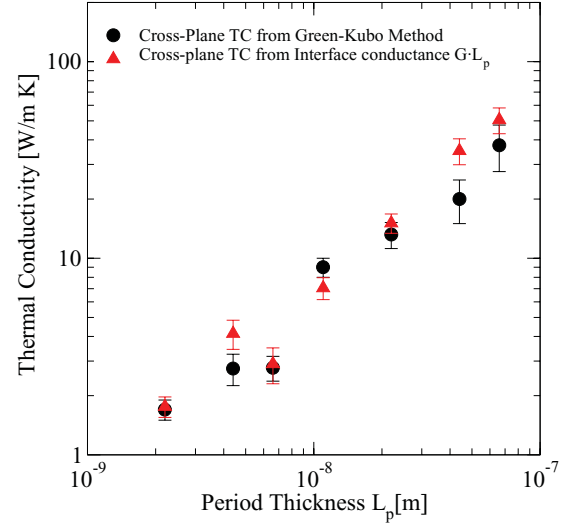


FIG. 8. (Color online) Computed thermal conductivity as a function of the layer thickness using the GK method and that derived from the contact resistance contribution.

In fact, lattice dynamics models overestimate coherence effects and neglect anharmonicity whereas the BTE only reproduces experimental results in the thick period range ( $L_p \gg \text{MFP}$ ). The purpose of this section is to propose and assess an effective cross-plane thermal conductivity model based on interface conductance and to compare it to the GK approach for defining to what extent cross-plane thermal conductivity of superlattices can be retrieved from interfacial conductance. As mentioned, we remain in a situation where internal phonon-phonon scattering is negligible. We used an effective thermal conductivity model where the thermal conductivity  $\lambda = GL_p$ ,  $G$  being the thermal conductance of the superlattice interface of period  $L_p$  retrieved from MD. To compare those results, we have implemented GK thermal conductivity calculations for period thickness ranging from  $\sim 2$  to  $\sim 60$  nm using the same equilibrium temperature as the thermal conductance calculations (400 K). Fifteen ensemble averages have been considered for each thermal conductivity point. Figure 8 shows that thermal conductivity of Si/Ge superlattices is fully driven by the interfaces' contribution below layer thicknesses of 5 nm. For larger thicknesses, ( $L > 10$  nm), we predicted a thermal conductivity of  $50 \text{ W/m K}^{-1}$  for a 60-nm-period superlattice whereas the GK method predicts  $40 \text{ W/m K}^{-1}$ . This seems to indicate that internal phonon-phonon scattering starts to occur in this regime.

The increase in thermal conductivity with increasing period is explained by a decreasing of the contact density (the number of interface per superlattice unit length) in the cross-plane direction. This behavior has also been observed by Daly *et al.*<sup>37</sup> and Chen *et al.*<sup>38</sup> We do not observe any saturation of thermal conductivity at thicker periods because they remain much smaller than the phonon MFP. One should expect such a saturation for periods larger than 100 nm. In conclusion, we have seen that thermal conductivity in perfect Si/Ge for system periods below the dominant phonon MFPs can be derived from interface resistances. In perfect materials with similar high phonon MFP, one should also expect an increase in thermal conductivity with increasing superlattice periods,

indicating that phonon-phonon scattering is negligible and coherence effects might be destroyed by inelastic scattering at the contacts.

## V. CONCLUSION

We formulated thermal interface conductance at the nanoscale within the framework of the linear response theory and presented an approach allowing us to retrieve thermal interface resistance from EMD simulations. Heat conduction mechanisms in various configurations of Si/Ge superlattices have been studied showing that temperature has no influence on phonon transmission. In addition, results clearly indicate that superlattice thermal resistance exhibits two trends with increasing period: Below 5 nm, thermal conductance decreases with increasing thickness because evanescent modes still exist over the full Si/Ge period. Above 5 nm, we observed a drastic decrease in conductance which no longer depends on thickness. Further confrontations with GK cross-plane thermal conductivity calculations demonstrated that thermal conductivity of Si/Ge superlattices can be deduced from inter-

face conductances when diffuse interface scattering occurs at periods exceeding 5 nm. Thus, thermal conductivity increases with increasing lattice periods as long as the dominant phonon MFP involved remains larger than the superlattice period. This indicates that interfacial scattering in perfect superlattices remains the predominant source of scattering in very large phonon MFP materials. It also demonstrates that coherency effects are not as important as expected in such systems where anharmonicity of interfaces seems to play a key role. An interesting extension of this work would be to include defects and roughness at the interface<sup>39</sup> and see how this affects interfacial conductance at various period thicknesses.

## ACKNOWLEDGMENTS

This material is based on work supported as part of the Solid State Solar-Thermal 150 Energy Conversion Center (S3TEC), an Energy Frontier Research Center funded by the U.S. Department of Energy, Office of Science, Office of Basic Energy Sciences, under Grants No. DE-SC0001299 and No. DE-FG02-09ER46577.

- 
- <sup>1</sup>V. P. Carey, G. Chen, C. Grigoropoulos, M. Kaviani, and A. Majumdar, *Nanoscale Microscale Thermophys. Eng.* **12**, 1 (2008).
- <sup>2</sup>D. Cahill, W. K. Ford, K. E. Goodson, G. D. Mahan, A. Majumdar, H. J. Maris, R. Merlin, and S. R. Phillpot, *J. Appl. Phys.* **93**, 793 (2003).
- <sup>3</sup>Y. Gao, A. Marconnet, M. Panzer, S. LeBlanc, S. Dogbe, Y. Ezzahri, A. Shakouri, and K. Goodson, *J. Electron. Mater.* **39**, 1456 (2010).
- <sup>4</sup>A. J. Minnich, H. Lee, X. W. Wang, G. Joshi, M. S. Dresselhaus, Z. F. Ren, G. Chen, and D. Vashaee, *Phys. Rev. B* **80**, 155327 (2009).
- <sup>5</sup>Y. C. Chen, M. Zwolak, and M. Di Ventra, *Nano Lett.* **12**, 1691 (2003).
- <sup>6</sup>S. P. Hepplestone and G. P. Srivastava, *Phys. Rev. B* **82**, 144303 (2010).
- <sup>7</sup>Y. Chalopin, J. N. Gillet, and S. Volz, *Phys. Rev. B* **77**, 233309 (2008).
- <sup>8</sup>Y. Chalopin, S. Volz, and N. Mingo, *J. Appl. Phys.* **105**, 084301 (2009).
- <sup>9</sup>E. T. Swartz and R. O. Pohl, *Rev. Mod. Phys.* **61**, 3 (1989).
- <sup>10</sup>N. Mingo and L. Yang, *Phys. Rev. B* **68**, 245406 (2003).
- <sup>11</sup>W. Zhang, N. Mingo, and T. S. Fisher, *Phys. Rev. B* **76**, 195429 (2007).
- <sup>12</sup>W. Zhang, N. Mingo, and T. S. Fisher, *Numer. Heat Transfer* **51**, 333 (2007).
- <sup>13</sup>L. Zhang, P. Keblinski, J. S. Wang, and B. Li, *Phys. Rev. B* **83**, 064303 (2011).
- <sup>14</sup>P. K. Schelling, S. Phillpot, and P. Keblinski, *Appl. Phys. Lett.* **80**, 2484 (2002).
- <sup>15</sup>B. Becker, P. K. Schelling, and S. R. Phillpot, *J. Appl. Phys.* **99**, 123715 (2006).
- <sup>16</sup>M. P. Panzer and K. E. Goodson, *J. Appl. Phys.* **103**, 094301 (2008).
- <sup>17</sup>Z. Y. Ong and E. Pop, *Phys. Rev. B* **81**, 155408 (2010).
- <sup>18</sup>P. Kubo, M. Toda, and N. Hashitsume, *Statistical Physics II* (Springer-Verlag, Berlin, 1985).
- <sup>19</sup>M. P. Allen and D. J. Tildesley, *Computer Simulation of Liquids* (Clarendon, Oxford, 1987).
- <sup>20</sup>N. Pottier, *Nonequilibrium Statistical Physics* (Oxford University Press, New York, 2010).
- <sup>21</sup>Mori *et al.*, *J. Phys. Soc. Jpn.* **11**, 1029 (1956).
- <sup>22</sup>G. Domingues, S. Volz, K. Joulain, and J. J. Greffet, *Phys. Rev. Lett.* **94**, 085901 (2005).
- <sup>23</sup>F. H. Stillinger and T. A. Weber, *Phys. Rev. B* **31**, 5262 (1985).
- <sup>24</sup>Zi Jian, Zhang Kaiming, and Xie Xide, *Phys. Rev. B* **41**, 12915 (1990).
- <sup>25</sup>S. Ethier and L. J. Levis, *J. Matt. Res.* **7**, 2817 (1992).
- <sup>26</sup>E. S. Landry and A. J. H. McGaughey, *Phys. Rev. B* **80**, 165304 (2009).
- <sup>27</sup>H. Zhao and J. B. Freund, *J. Appl. Phys.* **97**, 024903 (2005).
- <sup>28</sup>E. S. Landry and A. J. H. McGaughey, *J. Appl. Phys.* **107**, 013521 (2010).
- <sup>29</sup>S. Volz, J. B. Salunier, G. Chen, and P. Beauchamp, *Microelectron. J.* **31**, 815 (2000).
- <sup>30</sup>E. S. Landry and A. J. H. McGaughey, *Phys. Rev. B* **79**, 075316 (2009).
- <sup>31</sup>G. Chen, *J. Heat Transfer* **119**, 220 (1997).
- <sup>32</sup>E. S. Landry and A. J. H. McGaughey, *J. Appl. Phys.* **107**, 013521 (2010).
- <sup>33</sup>P. Hyldgaard and G. D. Mahan, *Phys. Rev. B* **56**, 10754 (1997).
- <sup>34</sup>G. Chen, *Phys. Rev. B* **57**, 14958 (1998).
- <sup>35</sup>P. Hyldgaard and G. D. Mahan, in *Thermal Conductivity* (Technomic, Lancaster, PA, 1996), Vol. 23.
- <sup>36</sup>S. G. Walkauskas, D. A. Broido, K. Kempa, and T. L. Reinicke, *J. Appl. Phys.* **85**, 2579 (1999).
- <sup>37</sup>B. C. Daly, H. J. Maris, K. Imamura, and S. Tamura, *Phys. Rev. B* **66**, 024301 (2002).
- <sup>38</sup>Y. Chen, D. Li, J. R. Lukes, Z. Ni, and M. Chen, *Phys. Rev. B* **72**, 174302 (2005).
- <sup>39</sup>K. Termentzidis, P. Chantrenne, and P. Keblinski, *Phys. Rev. B* **79**, 214307 (2009).